The Concentration Profile of Nitric Acid and Other Species over Saskatchewan in August 1998: Retrieval from Data Recorded by Thermal-Emission Radiometry

Brendan M. Quine[1*], Matthew Toohey[2], James R. Drummond[2], Kimberly Strong[2], Debra Wunch[2], Clive Midwinter[2] and C. Thomas McElroy[3]

[1]*Department of Physics and Astronomy, York University*
4700 Keele St, Toronto ON M3J 1P3
[2]*Department of Physics, University of Toronto, Toronto ON*
[3]*Meteorological Service of Canada, Downsview ON*

[Orginal manuscript received 22 August 2000; in revised form 29 June 2005]

ABSTRACT *We present vertical mixing ratio profiles for nitric acid (HNO_3) recorded during the Middle Atmosphere Nitrogen TRend Assessment (MANTRA) 1998 balloon flight over Saskatchewan, Canada. The profiles are based on radiance spectra containing HNO_3 thermal-emission features and were collected during balloon ascent and over a latitude and longitude interval (52°± 0.2°N, 106.6° ± 0.5°W) between 3:30 and 6:30 am local time (9:30 and 12:30 UTC), 24 August 1998. The spectra were simultaneously recorded by two radiometer instruments in the 715-1250 cm^{-1} atmospheric window at an approximate instrument resolution of 20 cm^{-1}. Profiles of CFC-11, CFC-12, ozone (O_3), methane (CH_4) and nitrous oxide (N_2O) based on emission features in the same observation window are also presented. Raw radiance measurements are analysed using a forward estimation technique to recover multiple gas profiles from very low-spectral resolution measurements of atmospheric radiance. The technique uses detailed atmosphere and instrument models and a least-mean-squares estimator to iterate maximum-likelihood volume mixing ratio (VMR) from 7 to 30 km on a 2-km grid. The analysis approach described is adaptable to other retrievals of multiple constituents from low-resolution spectra recorded by lower-cost, robust instrumentation developed for balloon and space flight. Averaging kernels and an error analysis are included in order to illustrate instrument sensitivity to vertical composition and expected accuracy. Results from each instrument compare favourably and show close agreement with HNO_3 climatology results based on satellite observations made by the Microwave Limb Sounding (MLS) instrument, 1992–94.*

RESUMÉ *[Traduit par la rédaction] Nous présentons les profils verticaux de rapport de mélange pour l'acide nitrique (HNO_3) enregistrés durant le vol de ballon de 1998 de l'Évaluation des tendances de l'azote dans l'atmosphère moyenne (MANTRA), en Saskatchewan, au Canada. Les profils sont basés sur les spectres de radiance affichant les caractéristiques d'émission thermique du HNO_3 et ont été captés durant l'ascension du ballon dans un intervalle de latitudes et de longitudes (52° ± 0,2°N, 106,6° ± 0,5°W) entre 3h30 et 6h30, heure locale (0930 UTC et 1230 UTC), le 24 août 1998. Les spectres ont été simultanément enregistrés par deux radiomètres dans la fenêtre atmosphérique 715-1250 cm^{-1} avec une résolution d'approximativement 20 cm^{-1}. Nous présentons aussi les profils du CFC-11, du CFC-12, de l'ozone (O_3), du méthane (CH_4) et de l'oxyde nitreux (N_2O) basés sur les caractéristiques d'émission dans la même fenêtre d'observation. Les mesures de radiance brutes sont analysées au moyen d'une technique d'estimation prospective pour extraire des profils de gaz multiples à partir de mesures de très faible résolution spectrale de la radiance atmosphérique. La technique utilise des modèles atmosphérique et instrumentaux détaillés et un estimateur des moindres carrés pour itérer le rapport de mélange en volume le plus vraisemblable de 7 à 30 km avec un pas de grille de 2 km. La méthode d'analyse décrite est adaptable à l'extraction d'autres constituants multiples à partir des spectres de basse résolution enregistrés par les instruments moins chers et robustes mis au point pour les ballons et les vols spatiaux. Les facteurs de pondération ainsi qu'une analyse des erreurs sont inclus pour montrer la sensibilité de l'instrument à la composition verticale et la précision attendue. Les résultats pour chaque instrument se comparent favorablement et affichent une bonne correspondance avec les résultats de la climatologie du HNO_3 basés sur les observations satellitaires faites par le Sondeur du limbe hyperfréquences (MLS), 1992-1994.*

1 Introduction

The 1998 Middle Atmosphere Nitrogen TRend Assessment (MANTRA) balloon mission was launched to examine the nitrogen budget of the stratosphere. The partitioning between active nitrogen species (NO_x = NO and NO_2) and total nitrogen (NO_y) is significant for chemical processes that deplete stratospheric ozone at mid-latitudes. Active nitrogen species

*Corresponding author's email: bquine@yorku.ca

can be converted into inactive forms that do not destroy ozone. One such important reaction,

$$OH + NO_2 \longrightarrow HNO_3, \quad (1)$$

converts ozone-depleting species OH and NO_2 into nitric acid which is a relatively inert reservoir species. In the lower stratosphere (below 30 km), it is expected that up to 90% of total nitrogen exists in the form of this reservoir species (see Chartrand et al., 1999). Despite its significance, nitric acid is only present in trace amounts in the atmosphere and typically comprises less than 10^{-8} by molecular density. Experimentally, the vertical composition has been probed by aircraft, balloons, and by satellite, but temporal and spatial coverage is sparse and, as we discuss, there is still significant measurement uncertainty.

This paper presents measurements of nitric acid concentration made by two emission radiometers with substantial flight heritage. Manufactured for the Atmospheric Environment Service of Canada (now the Meteorological Service of Canada) in 1985, at least forty instruments were built (see Ogston, 1991; Galbally, 1983). The Volume Mixing Ratio (VMR) vertical profile data collected with these instruments offer the best temporal coverage of any HNO_3 dataset—measurements made by these and similar instruments span nearly 30 years (see Evans et al., 1976, 1981, 1982a, 1982b). Two such instruments were included on the MANTRA 1998 mission, as part of an extensive instrumentation suite, for three reasons. Firstly, the instruments make localized observations compared with satellite instruments or balloon instruments using solar occultation; they also have high vertical resolution, enabling the spatial structure of atmospheric composition to be investigated. Secondly, the new flight data can be compared with the considerable archive of historical flight data taken by similar instruments. Thirdly, comparison of this technique and other approaches provides important continuity between measurement datasets.

Previously, flight-data analysis for the emission radiometers recovered nitric acid composition only. Smoothed vertical radiance profiles were estimated by binning radiance data at the spectral peak of nitric acid thermal emission. The VMR composition was then inferred from the differential change in radiance with respect to altitude (see Evans et al., 1976). This method is computationally efficient and extremely sensitive to vertical composition. However, our analysis indicates that the concentration profile generated by this method is directly correlated with the smoothing factor applied, and, consequently, the absolute VMR results are not reliable.

In this work, we present results based on the application of a maximum-likelihood estimation procedure that does not require profile smoothing. The approach employs a forward radiation model of the atmosphere and the radiometer instruments in order to predict instrumental response. A modern estimation technique is employed to estimate the VMR and instrumental parameters that best predict the observed radiance levels in a recursive optimization process that minimizes the least-mean-squares sum of the residuals in order to determine the most likely model fit to our data. We present profile results for two instruments, based on independent global optimization runs for each radiometer instrument that equally weights the value of spectral radiance data from a complete sequence of instrument scans. Our analysis also extends the number of gas species recovered from each instrument from one to six.

The following sections discuss the MANTRA mission and the radiometer instrument. The previous technique used for the analysis of emission radiometer data is discussed, and the new technique is introduced. Results from the emission radiometers are presented along with HNO_3 climatology results based on Microwave Limb Sounder data collected by the Upper Atmosphere Research Satellite (UARS) (1992–94) and the Fourier Transform Infrared Radiometer (FTIR) data collected during the same balloon flight. Averaging kernels and an error analysis are included in order to illustrate instrument sensitivity to vertical composition and expected accuracy.

2 The MANTRA mission

The 1998 MANTRA balloon flight was launched from Vanscoy, Saskatchewan, at approximately 3:25 am (09:25:25 UTC) on 24 August 1998. An overview of the MANTRA mission is given by Strong et al. (this issue). The balloon carried two emission radiometers making spectral emission measurements in the 8–14 μm region. One instrument recorded spectra with a field-of-view elevation of 19.0°, and a similar instrument made measurements at 41.0°. The instrument-viewing geometries are illustrated in Fig. 1. The radiance spectra were collected while the balloon ascended over a latitude and longitude interval (52° ± 0.2°N, 106.6° ± 0.5°W) and between 09:30 and 12:30 UTC, 24 August 1998. This paper presents VMR results for six gases as analysed from this flight data.

The mid-latitude August launch provided an ideal opportunity to study nitric acid. Diurnal variations in nitric acid concentration are small, and chemical transport models predict particularly stable stratospheric concentrations for this period and latitude.

3 Instrument description

Emission radiometers were first developed by Pick and Houghton (1969). The instruments consist of an insulated liquid-nitrogen dewar containing a cooled detector and optics and originally made measurements of the atmospheric thermal emission in the 10.3–12.5 μm (800–970 cm^{-1}) region. The instruments employ reflective optics to maximize signal intensity and to simplify radiometric calibrations. A 200-Hz mechanical chopper modulates the detector signal at the entrance slit. Incoming radiation is passed though a filter and is focused onto a mercury-cadmium-telluride detector. A low-noise linear preamplifier amplifies the detector signal. The instrument produces low and high-gain output channels via independent linear amplifiers and associated phase-sensitive detectors.

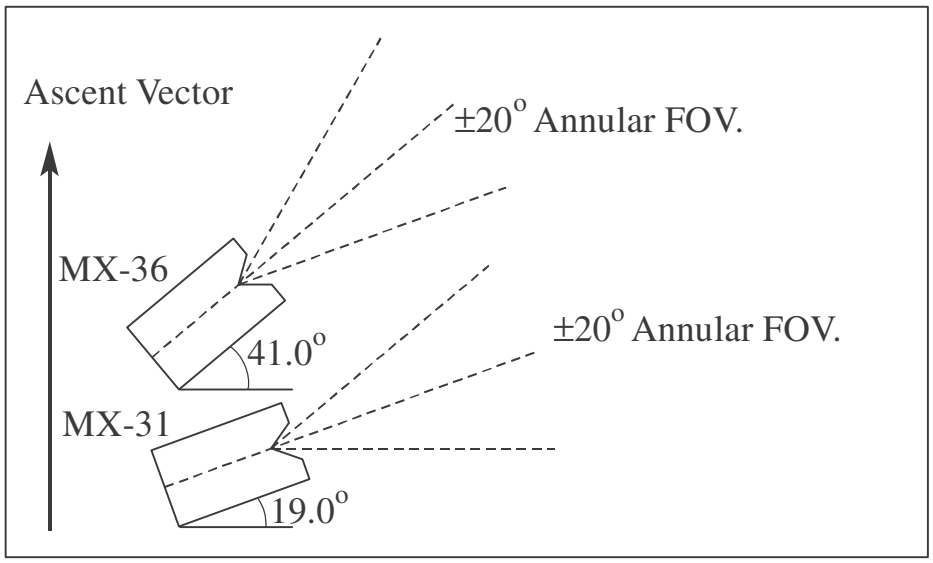

Fig. 1 Instrument fields of view (FOV).

A Canadian version of the instrument was developed by Evans et al. in the early 1970s (Evans et al., 1976). The early instrument design employed five discrete band-pass filters to sample overlapping sections of the nitric acid bands ν_5, $\nu_5 + \nu_9 - \nu_9$ and $2\nu_9$. Radiance estimates were derived from band-pass measurements of this region (centred on 11.3 μm or 885 cm^{-1}) and a careful filter calibration. A later instrument design, used in this work, replaced the discrete filters with continuously variable filter (CVF) segments (Morelli, 1998). With two segments mounted on a continuously turning wheel, these instruments scan a wavelength region from 8–14 μm (715-1250 cm^{-1}) with a pass-band width varying between 1% and 4% of the centre wavelength (approximately 20 cm^{-1} at 884 cm^{-1}). This later instrument design also includes a filter-wheel location encoder to ensure scan-to-scan repeatability and to provide a means for calibrating the frequency axis. The instrument is operated in a continuous scan mode, completing each scan cycle in 40 seconds. Part of the filter wheel is blanked off, providing a background radiometric calibration for each scan.

The instruments have a wide torroidal field of view with a sensitivity extending over a ±20° range with peak sensitivities at ±10°. A correction factor for the slant path elevation angle is computed for each instrument to account for this variation using an experimentally derived angular sensitivity function. The function is verified by an angular characterization of the instrument with a hot narrow source but shows little inter-instrument variation.

The instrument also includes a blackbody calibration flap that is automatically lowered to cover the field of view every five scans. The flap, mounted externally to maintain a temperature above that of liquid nitrogen, has an embedded platinum resistance thermometer to provide an in-flight radiometric calibration. Figure 2 illustrates this later instrument design.

Traditionally, the instrument is mounted on a balloon payload in an anti-sun pointing configuration at an elevation angle of approximately 20° above the horizon resulting in an increased atmospheric slant path. Measurements of the atmospheric radiance profile are made during the ascent phase of a balloon mission. This flight carried two emission radiometers (serial numbers MX31 and MX36). Since the hardware design had considerable flight heritage, only minor modifications were made to the original configuration in order to improve cryogen life and the in-flight calibration procedure.

The simultaneous flight of two nearly identical instruments allowed for an assessment of inter-instrument variability. The instruments were operated continuously during ascent with one instrument (MX31) mounted at 19.0° elevation and the other (MX36) at 41.0°. This ensured that the instruments had independent spatial and temporal atmospheric paths. The configuration also allowed for an assessment of the effect of payload swing on measurements (the lower-elevation instrument would be approximately three times more susceptible to pendulum-like motion than the higher-elevation instrument due to the gearing of the slant path with elevation angle). The corresponding geographical sampling intervals are estimated to be 2° and 1° (2 sigma) of spherical surface for the two instruments, respectively.

4 Emission radiometry

The radiometer measures the cumulative spectroscopic gas emission in the 8–14 μm (715–1250 cm^{-1}) atmospheric window along an upward-looking slant path. At the beginning of the ascent, the instrument views a slant path through the whole atmosphere, and radiance measurements are at a maximum. The instrument ascends through the atmosphere, continuously scanning the spectral window and acquiring new radiance measurements at a series of altitudes. As the instrument rises,

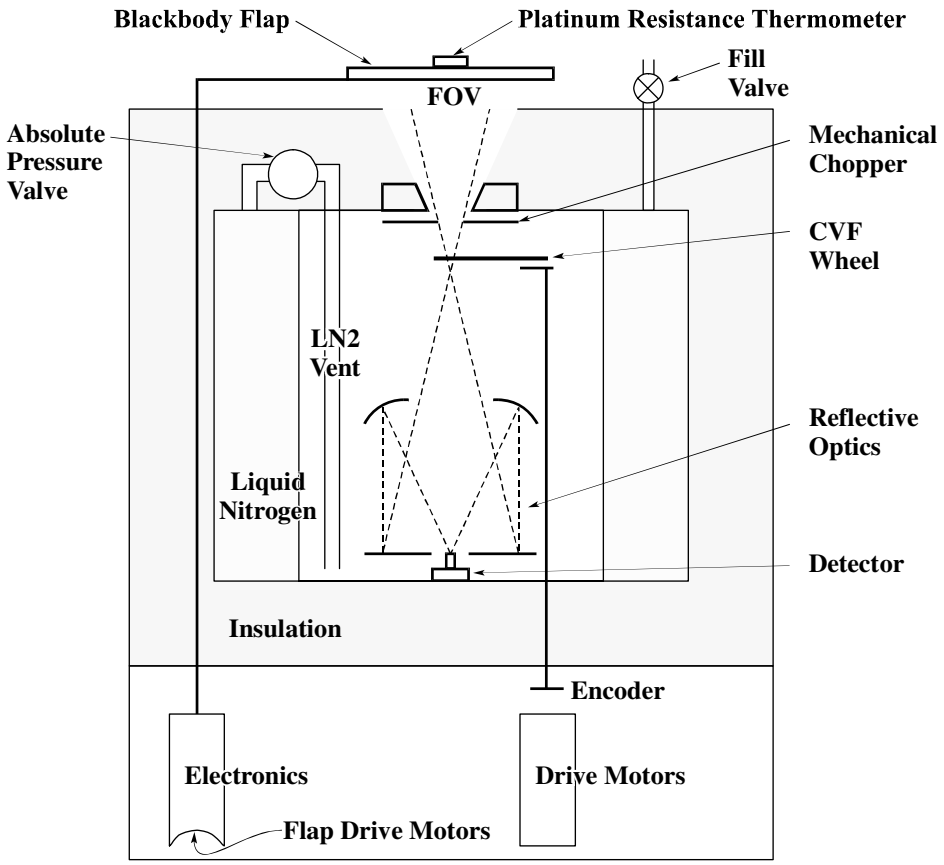

Fig. 2 Schematic of the radiometer instrument.

the atmosphere below the instrument is excluded from the slant path, making these instruments extremely sensitive to vertical composition. Assuming that the atmosphere is approximately horizontally stratified, the emission of individual atmospheric layers (between the initial and final altitudes) can be inferred from the set of scans. In the absence of significant scattering and assuming a Beer-Lambert radiative transfer model, these radiance measurements can be converted into gas amounts (or VMRs).

5 Instrument calibration

The instruments are calibrated in flight using a blackbody calibration source equipped with an embedded platinum resistance thermometer, calibrated prior to flight, that monitors flap temperature. The in-flight calibration source has not been utilized in previous analyses as it had been observed that the blackbody flap cooled significantly during calibration scans. This cooling (of approximately 4 K) is attributed to instrument out-gassing of the liquid nitrogen cryogen through the field-of-view port, necessary to keep the instrument optical path at liquid nitrogen temperatures. An error in blackbody calibration temperature translates into approximately a 2% K^{-1} error in calibrated radiance. In addition, the flap temperature is only sampled to 1 K accuracy, introducing quantization error.

The previous problems with in-flight calibration were overcome in two ways. Firstly, the instrument blackbody flaps were thickened to increase thermal inertia. This reduced the temperature change to about 1 K during a blackbody scan. Secondly, a temperature trend was interpolated from the flap-temperature data during each calibration scan. Since the temperature was changing during each scan, it was possible to recover a temperature-trend estimate to a precision that exceeded the data quantization by an order of magnitude. Figure 3 shows the flap-temperature data during one flight calibration scan as a function of the filter-wheel encoder value and the subsequently interpolated trend. When applied to all the flight calibration scans, the results of the radiometric calibration are remarkably consistent. Figure 4 shows that the radiance calibration parameter for a particular spectral sample varied monotonically with altitude. The detector and optics are cooled by liquid nitrogen out-gassing. This cooling is correlated with the ambient pressure and therefore shows an altitude dependency.

Use of in-flight calibration has significant advantages over the previous pre-flight and post-flight calibration strategy. Firstly, calibrations are made under instrument conditions identical to those of the flight measurements, and there is no need for an additional pressure-correction calibration since calibrations for each instrument scan can be directly interpolated from the in-flight calibration scans. There is evidence that, even after accounting for macroscopic changes with pressure, small variations in instrument response occur during flight and are captured by the in-flight calibration. Secondly, there

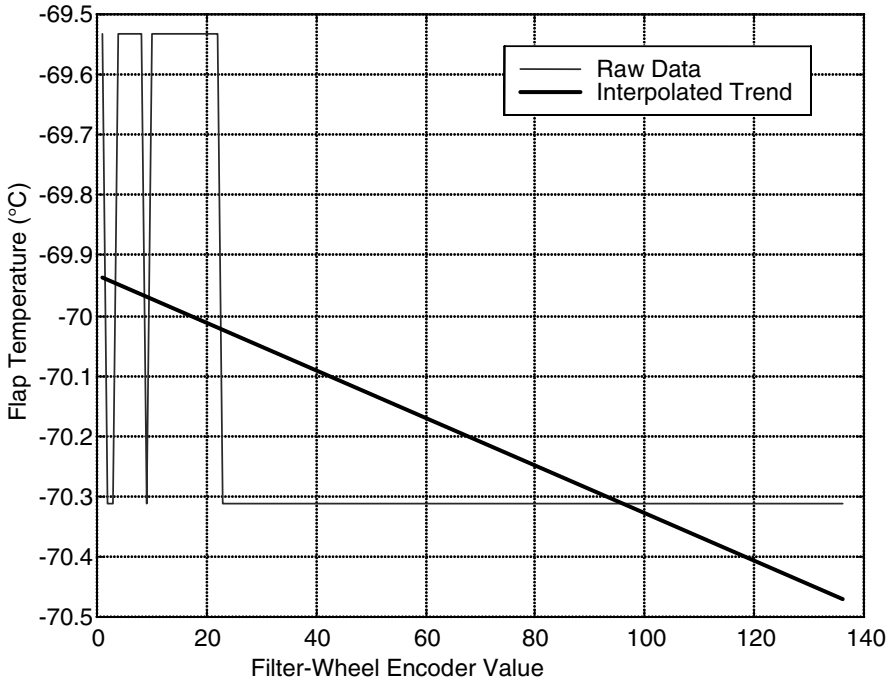

Fig. 3 Interpolating a blackbody flap-temperature trend for in-flight calibration.

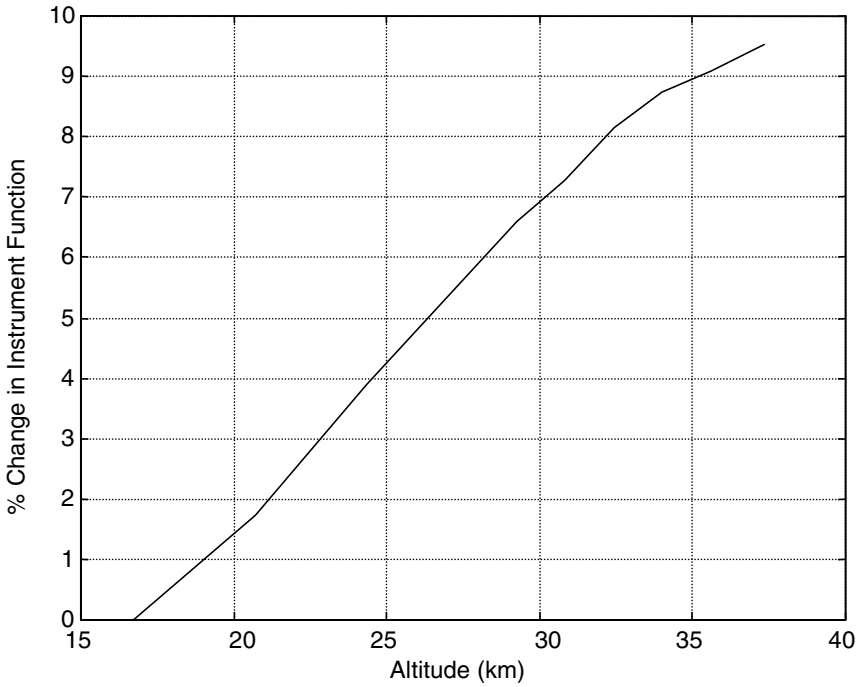

Fig. 4 Variation in instrument response at 884 cm^{-1} (MX-31, at peak of nitric acid emission).

is no need for extensive pre-flight and post-flight calibrations. As one instrument was damaged during the MANTRA flight, a post-flight calibration was impossible.

6 Previous analysis techniques

Evans et al. (1976) developed the previous analysis used to recover profile information for the original instruments in the early 1970s. Raw instrument data are converted into calibrated radiance data using blackbody and pressure-variation corrections recorded during extensive pre-flight calibrations. Layer emissions for nitric acid are determined by first smoothing the altitude-radiance dataset using a triangular filter (typical half-width 3 km) and then numerically differentiating the smoothed data and applying band parameters

(Goldman et al., 1981) to determine layer amount. With knowledge of layer temperatures and pressures, the layer-emission values are directly converted into layer-gas amounts and VMRs. Figure 5 shows the results of this analysis applied to one of the MANTRA flight instruments. The approach is computationally efficient (flight data can be analysed by hand) and is extremely sensitive to vertical structure. However, it suffers from a number of weaknesses:

- Only radiance measurements at 885 cm^{-1}, out of 600 spectral samples in each scan, are used in the analysis.
- The analysis will only recover profiles of nitric acid and cannot easily be extended to include other gases that are not spectrally isolated at the instrument frequency resolution. Roselli (1977) had previously applied a band-model retrieval technique to the measurement of ozone from the strong 9.6 μm emission band, but this analysis was of limited success and was never adopted in subsequent work.
- The VMR computed depends on the degree of smoothing applied because smoothing operations act to decrease the differential and, consequently, estimates of the peak nitric acid concentration are not reliable. Figure 6 illustrates how the nitric acid peak amount varies with smoothing filter half-width applied.
- The technique is deterministic and generates no residuals to indicate how well the atmospheric model assumptions fit the observed radiance data. It is therefore not possible to discriminate between real structure in the VMR profiles and those contributed by the profile-retrieval analysis.
- The technique does not include temperature dependence for the nitric acid band-line strengths. Instead, a single coefficient that describes the band-absorption coefficient is employed.

Applying the analysis to this flight, we also found a 30% discrepancy in the peak concentration of nitric acid recovered from the two MANTRA instruments when the data were analysed using this approach. For these reasons, a new technique was developed for the MANTRA flight analysis and is described in the following sections.

7 New analysis technique

The new analysis is based on realistic *predictive* or *forward* models of the atmosphere and instrument. These models, given expected gas amounts, atmospheric temperature and pressure information, and some instrument-calibration parameters, predict the expected instrument observations recorded in flight. Calculating a measurement residual (the difference between the actual measurements and the predicted measurements), a variety of estimation techniques can be applied to iterate for the underlying VMR profiles. Most simply, a least-mean-squares optimization criterion and gradient driven Levenberg-Marquardt solution search can be applied to find the best global fit; however, the performance of this derivative-based approach is poor in the optimization of problems with experimental noise as it will tend to converge to local minima. Here, a modified Nelder-Mead technique is employed that does not rely on derivatives and is particularly suitable for the optimization of large-scale, non-linear problems with non-smooth objective functions. The analysis proceeds as follows:

(1) The spectral response of the atmosphere is computed based on a model of the MANTRA atmosphere comprising discrete cells on a vertical grid. A 2-km grid is used so that altitude intervals are large enough to ensure that there are one or more scans within each spectral interval. For each cell, a mean temperature and pressure are determined using the Curtis-Godson approximation. Absorption coefficients are calculated in advance for each cell and for each gas using the GENSPECT line-by-line code, and assuming a Voigt line-shape model (Quine and Drummond, 2002). Line data in the 11-μm region are based on measurements recorded in the HITRAN database (Rothman et al., 2003) and reported by Goldman et al. (1998). Line intensities in this region may require further scaling by $1.14 \pm 6\%$ for ν_5, and $2\nu_9$ bands and 0.967 for the $\nu_5 + \nu_9 - \nu_9$ hot band Q-branch (see Toth et al., 2003), however, the broad spectral sampling of the radiometers will reduce the error of this measurement bias. Since pressure and temperature were not directly measured during the MANTRA 1998 flight, this information is interpolated from ozonesonde flights conducted before and after the main launch, using Global Positioning System (GPS) altitude data from the main flight. Absorption coefficients are calculated at 0.002 cm^{-1} resolution and then averaged and decimated to 0.01 cm^{-1}. This decimated grid has a relatively high resolution compared with that of the instrument (approximately 2000 times higher), but this resolution is required to ensure that emission energy and integrated line strength are adequately preserved. For these retrievals, eight gases are considered as contributing to the emission and are included in the model. They are HNO_3, CO_2, O_3, N_2O, CFC-11, CFC-12, H_2O and CH_4.

(2) The raw spectral data are recovered from flight telemetry, and each packet is verified for data integrity and to remove packet fragmentation caused by telemetry dropout. Calibration scans are identified, and these spectra are compared with synthetic blackbody spectra, generated using the calibration source temperature during the flight, in order to estimate absolute radiance-calibration factors as functions of flight time and spectral interval. Further details of the temperature calibration are provided in the next section.

(3) The VMRs are crudely initialized to values given by Salby (1996), and the radiation field for a slant path at each model level is estimated. The slant path angle is estimated from the instrument mount angle measured before launch, weighted by the instrument apparatus function.

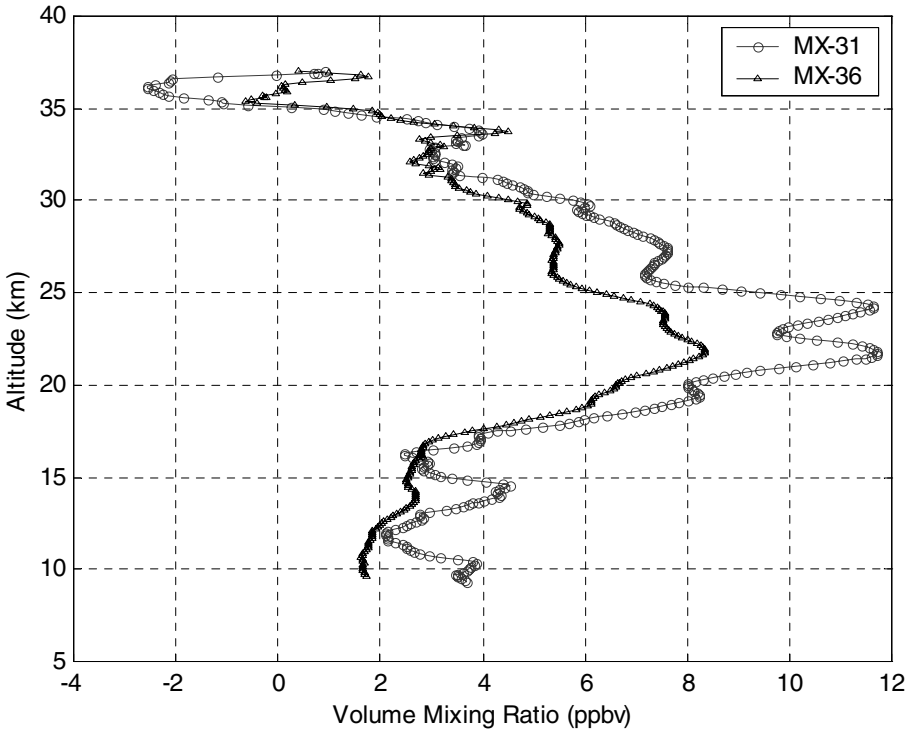

Fig. 5 Retrieved nitric acid VMR using old analysis technique with 3-km smoothing filter width.

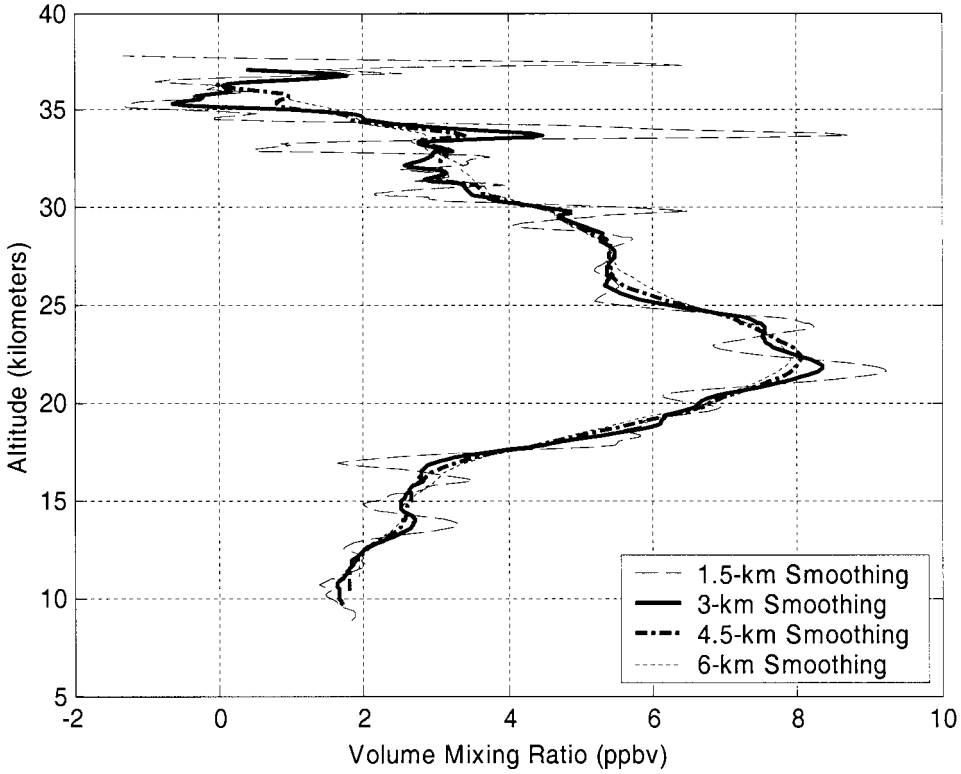

Fig. 6 Variation as a function of smoothing filter half-width for MX-36 (old analysis technique).

The strong ozone absorption feature (950–1150 cm^{-1}) was excluded from the retrieval analysis as it is difficult to model atmospheric transmission accurately in regions of optical opacity. In these regions, strong gas lines saturate before weaker lines, and only an atmospheric model that includes no frequency averaging can capture this

behaviour. Any such averaging would act to smooth out the strong line features, attenuating their saturation. Retrieval calculations are restricted to two windows on either side of the strong ozone-absorption feature, where the transmission is non-zero. HNO_3, CFC-11, and CFC-12 are recovered principally from an 850–950 cm^{-1} atmospheric window, and ozone, N_2O, and CH_4 are recovered principally from an 1150–1250 cm^{-1} atmospheric window. CO_2 and water vapour were included in the retrieval as minor emission species, and their VMRs were fixed according to results from the Canadian Middle Atmosphere Model (Chartrand, personal communication, 1999). Figure 7 shows radiance measurements with fit residuals for a range of altitudes.

(4) After calculating the expected atmospheric emission at each atmospheric level, the radiance estimates are then convolved with the instrument's slit function to produce a spectral response representative of the instrument. The slit function is itself a convolution of two components: a Gaussian function representative of the spectral response is convolved with an exponential function that accounts for the instrument's temporal sampling as the filter rotates in front of the detector. A Gaussian form for the spectral response function is initialized to parameters derived from experimental data provided by the variable filter manufacturer (Morelli, 1998) and retrieved in subsequent optimization. The form and time constant for the exponential temporal sampling function is determined by the instrument sampling electronics and filter rotational rate. Since the two slit function components scale differently with wavelength, an individual slit function is calculated for every spectral sample used in the retrieval. The instrument response at each spectral interval in time is estimated by interpolating convolved spectra onto the instrument spectral interval using a linearly varying wavelength calibration, which is also retrieved during subsequent optimization. The spectra are converted from standard radiance units into the instrument's radiance units using the instrument sensitivity function calculated in step (2) and interpolated from the 2-km grid to each measurement altitude. The conversion of calibrated radiance data into the instrument measurement units enables the optimization to proceed in the instrument observation space where a linear measurement noise model may be applied. The significance of each element of the measurement set is weighted equally in the optimization assuming that a quantifiable and random stochastic noise process corrupts the measurement sequence. Analysis of blackbody scans indicates that this noise model is valid during the period of the data acquisition, but the approximation will no longer hold if measurements are first converted by multiplication with a non-linear, instrument-sensitivity function to standard radiance-unit space.

(5) A residual difference between the real and the synthetic observation sets is computed. A Nelder-Mead type estimator (Nelder and Mead, 1965) with additional random jitter estimates the composition profiles for six gases simultaneously on a 17-layer vertical grid by recursive evaluation of the atmosphere and instrument models described in steps (3) and (4). The solution space is bounded to within a four order-of-magnitude range (by gas) centred on the expected mixing-ratio solution. In addition, two slit-function widths and four frequency-calibration parameters are simultaneously retrieved, giving a total of 108 parameters in the non-linear forward model. The optimization commences with a sub-optimal, top-down or onion-peeling search (Gille and House, 1971) to refine values before the global optimization is applied. The use of a forward estimation is computationally intensive compared with traditional techniques but provides the only means with which to search for a globally optimal solution in non-linear problems. Steps (3) and (4) require approximately 10^7 calculations per iteration, and the estimator requires of the order of 10^4 cycles to converge, taking 50 hours of processing time on a Pentium II 450 MHz platform. The generation of estimate residuals in this process adds significant value to the profile estimates by providing an indication of how well model assumptions fit the experimental regime and is invaluable to accurate error analysis.

8 Flight results and intercomparison

Both radiometer instruments performed nominally throughout the MANTRA 1998 flight, each collecting approximately 140 spectral scans of data during the balloon's ascent phase. There was, however, loss of data during the first twenty minutes of flight due to telemetry problems, but this data loss occurred at altitudes below 10 km, where atmospheric saturation prevents useful data analysis.

Analysed results of HNO_3 VMR for both instruments are shown in Fig. 8. Recovery of the HNO_3 profile is good, with both instruments reporting similar values over a wide altitude range. The radiometer results reported are sampled over the surface-interval 51°–53°N and 106°–108°W including field-of-view effects. The consistency between the two instrument profiles and fit residuals indicates that balloon swing was not a significant factor. The profiles show some difference between the altitudes of 7 and 22 km, which is larger than the expected experimental error and is likely attributable to the difference in air masses sampled by the two instruments, induced by their different viewing geometries. Schneider et al. (1998) report variations between 0.2 and 1.1 ppbv in HNO_3, over the interval 49°–51°N, recorded by mass spectrometer during long duration aircraft flights between the altitudes of 10 and 11 km in July 1996. Our results also indicate that there may be significant horizontal and vertical structure to the HNO_3 field and we recover a variation range consistent with these aircraft measurements.

Figure 8 also includes climatological HNO_3 profiles retrieved from Microwave Limb Sounding (MLS) data between 1992 and 1994 (Santee et al., 2004) and binned over 52.1°–53.1°N in August and September, as well as profiles

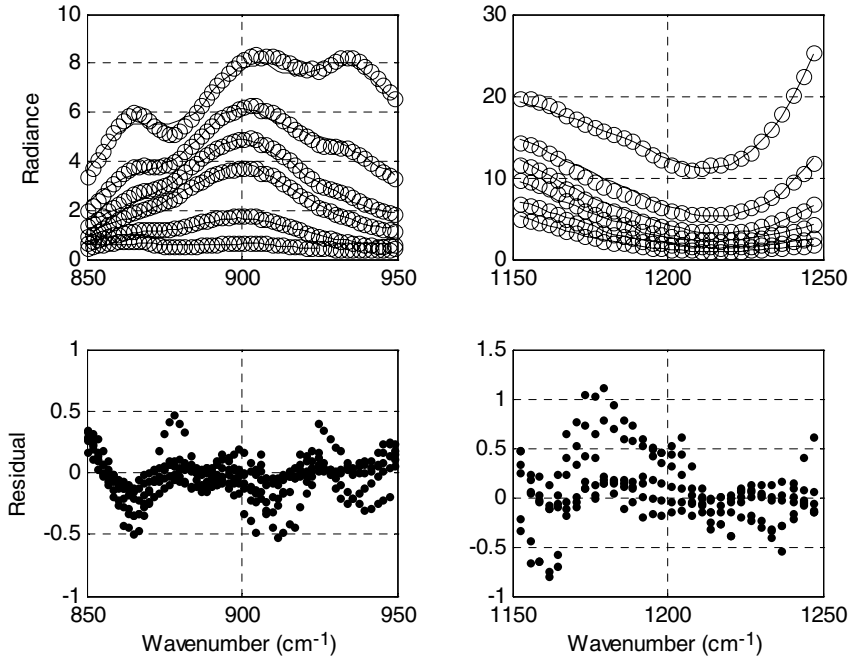

Fig. 7 Measured radiance and fit residual for the regions surrounding the strong ozone absorption (950–1150 cm^{-1}).

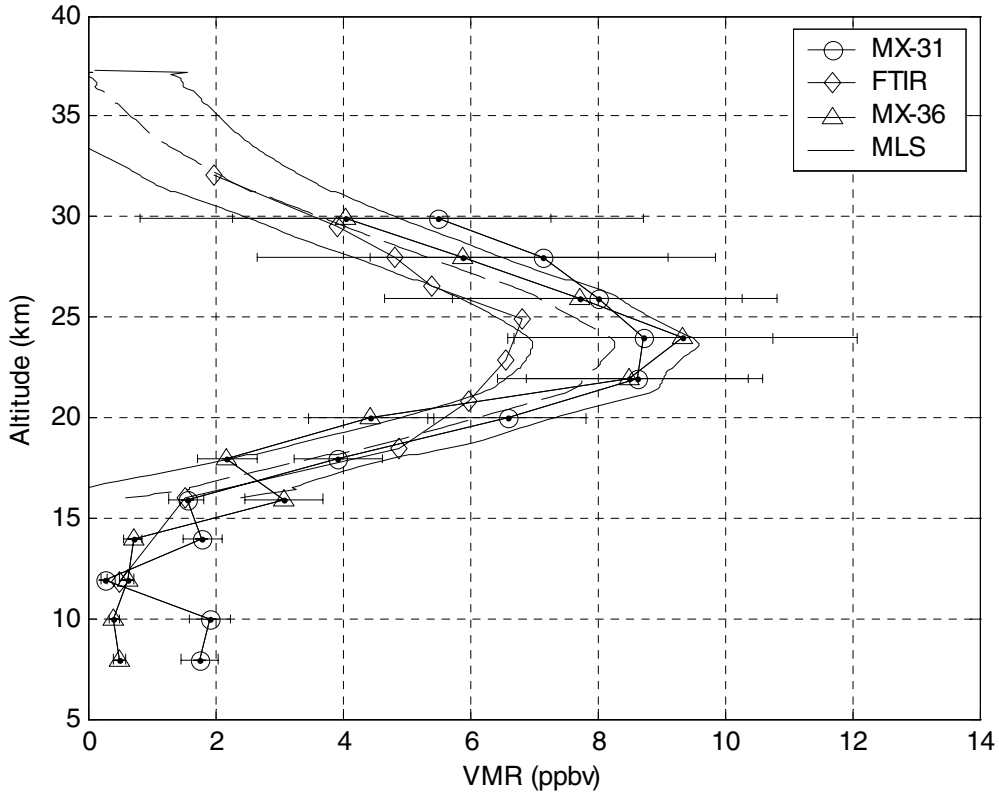

Fig. 8 VMR profile for HNO_3. Averaged MLS data are shown for HNO_3 with one-sigma variability lines (FTIR data, Fogal et al. (this issue), MLS from Santee et al., 2004).

based on solar occultation measurements recorded by the Fourier Transform Spectrometer (FTIR) during the MANTRA flight and reproduced here for comparison (Fogal et al., this issue). Our data show close agreement with the zonally averaged MLS results for this season. Previous satellite-balloon intercomparisons (Kumer et al., 1996) have

reported a discrepancy of more than 20% for HNO_3 profile results during a Cryogenic Limb Array Etalon Spectrometer/Fourier Transform Spectrometer (CLAES/FTS) intercomparison campaign in 1992.

Results from the radiometers also compare well with those made by FTIR up to an altitude of 18 km, although the FTIR reports peak nitric acid VMR as approximately 20% lower than the values retrieved here between 20 and 30 km. Significant differences in the air masses sampled by the two approaches may explain this difference. The FTIR spectra are recorded during sunrise at low elevation, and by geometrical argument their typical sampling interval is of the order of twice the solar elevation angle during measurement. Consequently, scans collected during sunrise at –5° elevation will be sampled over a 10° angular interval in an azimuth direction of 95°. Latitudinal gradients in HNO_3 column amount with low concentrations of HNO_3 at the equator and high concentrations in polar regions have been reported previously by Gille et al. (1984a, 1984b) and Murcray et al. (1987), based on a compilation of space and balloon-based measurements. They report column gradients of between 1% and 5% per degree latitude at 50°N, depending on the season. Santee et al. (2004) report a similar latitudinal variation and also present polar contour maps of HNO_3 concentration that indicate significant longitudinal structure in the HNO_3 field even at 400-km spatial resolution, providing a likely explanation for the lower peak amount reported by the FTIR. Further, both FTIR and MLS data are recorded over transmission paths that vary horizontally with altitude, and profile information is reconstructed in subsequent data analysis. Consequently, the retrieved profiles are likely more susceptible to layer-smoothing effects, which would reduce the peak emission. In contrast, the radiometer data are recorded at high vertical resolution, and, consequently, the retrieval is less susceptible to the vertical smoothing of composition profiles. Independence between retrieved quantities at each vertical layer was tested through the computation of diagnostic averaging kernels. An averaging kernel matrix, **A**, was calculated numerically by finding the change in the retrieved HNO_3 profile which resulted when each element of the final retrieved HNO_3 profile was perturbed by 10%. The difference between the original and subsequently retrieved profile, divided by the change in the state profile, was then recorded in the appropriate column of the **A** matrix, whose rows then provide the averaging kernels. When this analysis was applied to the first guess estimate retrieval, the resultant averaging kernels, shown in Fig. 9, exhibit delta-function behaviour at each retrieval layer as a consequence of complete independence between layers.

Weighting functions were also calculated as a retrieval diagnostic, and to test the forward model. Figure 10 shows a selection of weighting functions over the full set of atmospheric scans made by the MX-31 instrument during the balloon ascent. These weighting functions represent the change in forward modelled radiance at the peak HNO_3 emission corresponding to a 10% change in the HNO_3 profile at each model layer height, over the series of all measurement altitudes. At all retrieval altitudes, the largest source of measured radiation is from the model layer directly above the retrieval altitude. As the instrument ascends, atmospheric layers below the instrument altitude do not appear to contribute to the observed radiance. The exponential decrease in the magnitude of the weighting functions with altitude is a direct result of the exponential decrease in gas density with altitude.

The VMR results for ozone are shown in Fig. 11. Ozone is harder to recover than HNO_3 since the gas is an extremely strong absorber and can therefore only be estimated at the edge of the main absorption band. The MX-31 instrument gives results that are very close to those measured by ozonesonde flights launched within twenty-four hours before and after the main payload launch. The results are also similar to those of the FTIR, although the FTIR reports an enhancement at 30 km. The MX-36 instrument results are also similar in overall profile, although the instrument reports a secondary peak at 23 km and a local minimum at 26–28 km. The ozonesonde instruments also report smaller enhancements in ozone concentration at 23 km. It is possible that these results indicate that the ozone field also exhibits significant inhomogeneity that may have been smoothed during sample collection by in situ sampling instrumentation because of balloon-induced turbulence and chemical reaction delay.

Results for CH_4, N_2O and CFC-11 and CFC-12 are presented in Figs 12 and 13 with the FTIR results included for comparison. Despite significant overlap in spectral emission features and a reduced instrumental sensitivity to these species compared with HNO_3, composition profiles are generally well recovered. As with HNO_3, the radiometers report mixing ratios that are generally higher than those recorded by the FTIR. The profiles also exhibit considerable structure that is present in the raw radiance record and consistent between radiometer datasets.

9 Error analysis

The retrieval algorithm includes a sensitivity and error analysis to calculate estimated error bars for each gas-mixing ratio at each altitude point. After the estimator has converged to produce a set of best-fit mixing ratios, a sensitivity ratio is computed. Working sequentially by gas, the best-estimate mixing ratio is perturbed by 1% in order to determine the reciprocal change in radiance at each atmospheric layer: this defines the sensitivity ratio. The percentage fit error is then calculated for each spectral sample at each measurement height as the typical fit error (0.4 for MX-31 and 0.25 for MX-36 in units of counts divided by 3.2766×10^3). By dividing the percentage-fit error by each gas-sensitivity ratio an estimate of expected percentage errors are determined by gas, by spectral sample, and by altitude. A conservative estimate of percentage error by altitude and by gas can then be determined from the spectral sample at which each gas is best recovered.

Although this analysis is not strictly rigorous, it nevertheless gives a good indication of how well each gas can be retrieved. An additional 14% root mean square (r.m.s.) error term is added to these results to account for errors in radiance calibration (10%) and errors in line-strength data (10%).

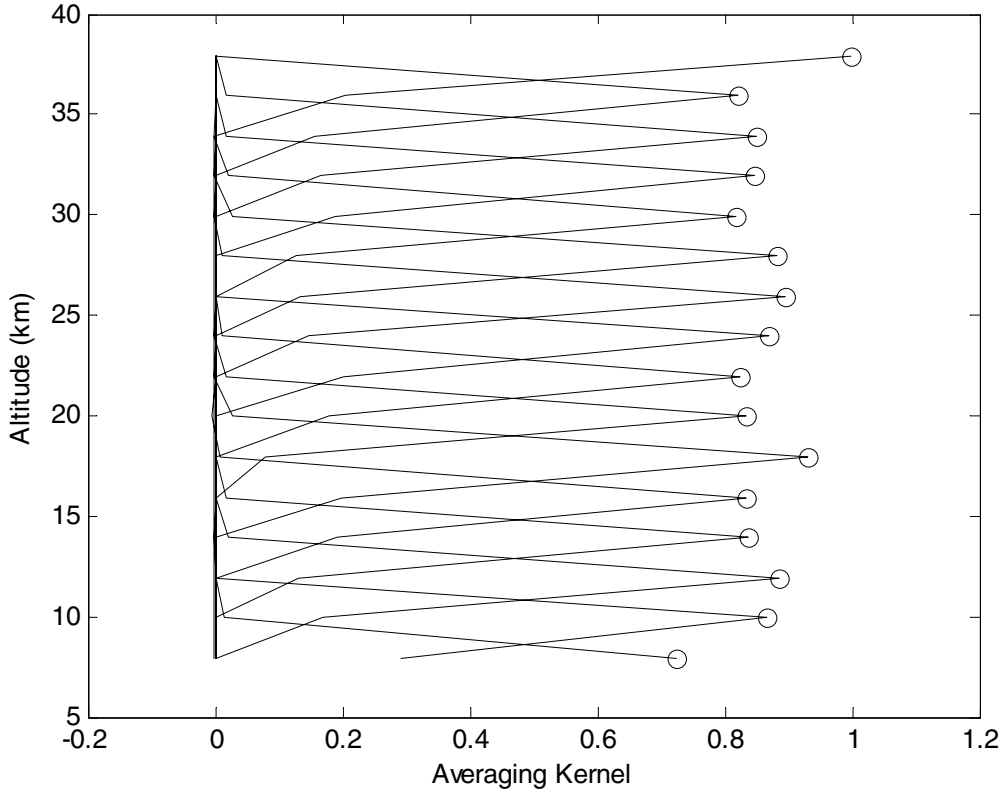

Fig. 9 HNO_3 averaging kernels computed for Radiometer MX-31 indicating the altitude sensitivity of each retrieval layer.

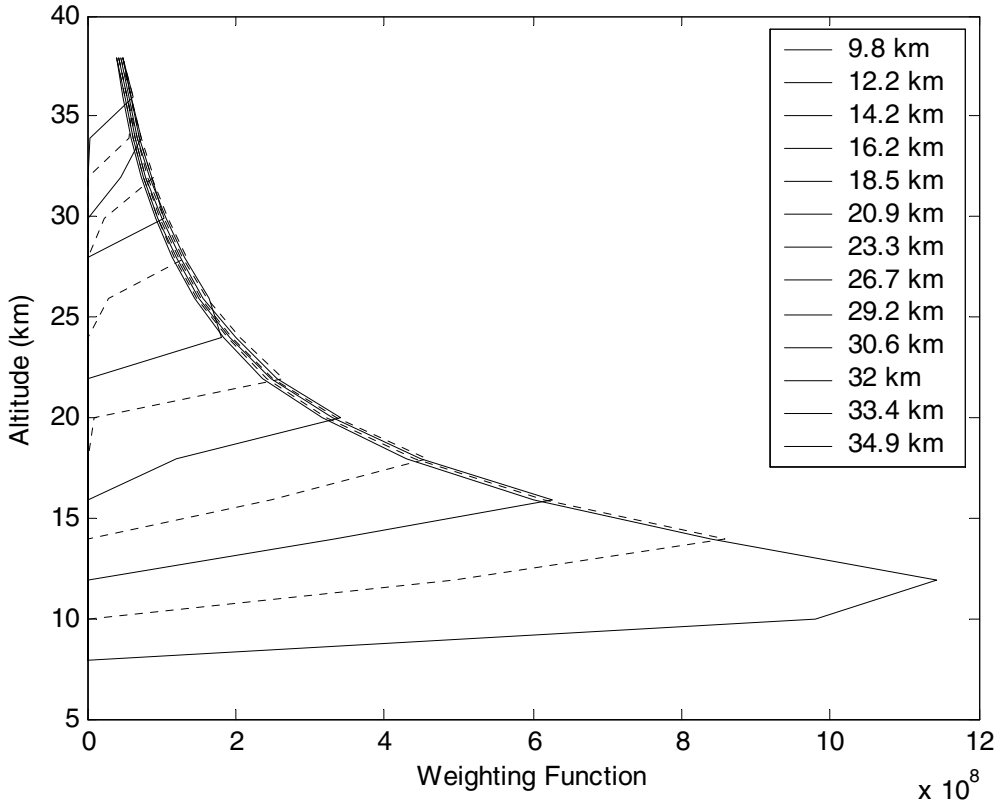

Fig. 10 HNO_3 weighting functions for the atmospheric model deployed in the retrieval analysis.

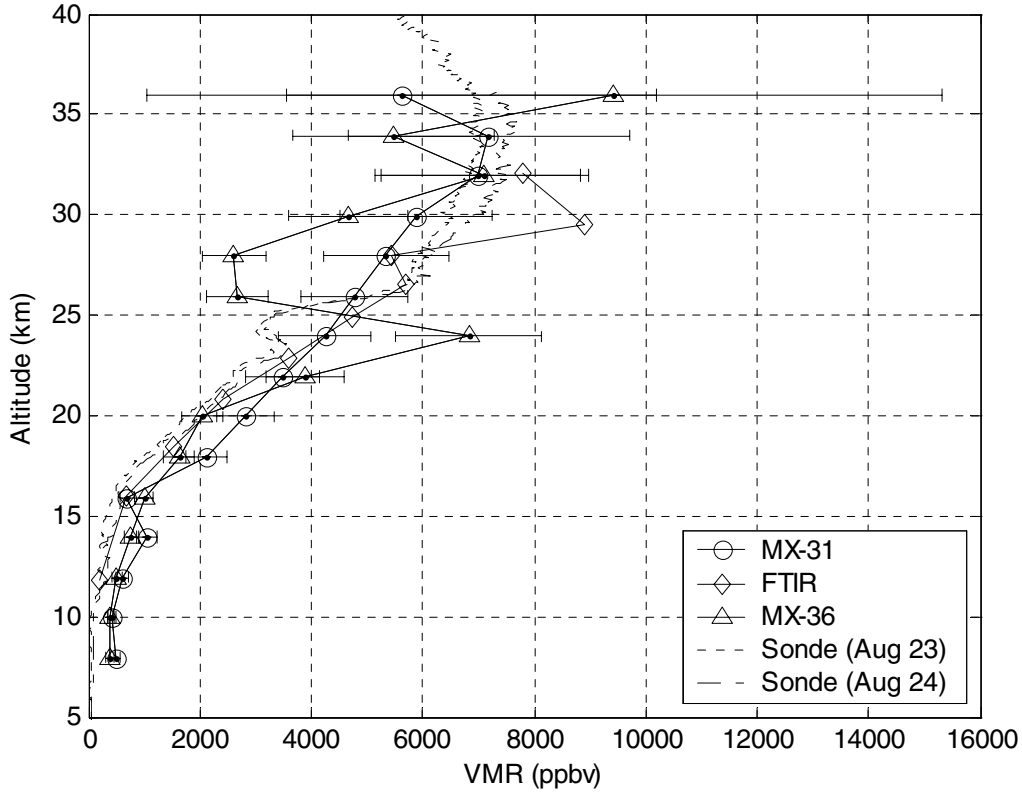

Fig. 11 VMR profile for ozone, FTIR data, Fogal et al. (this issue), sonde data courtesy Davis (personal communication, 1999) of the Meterological Service of Canada.

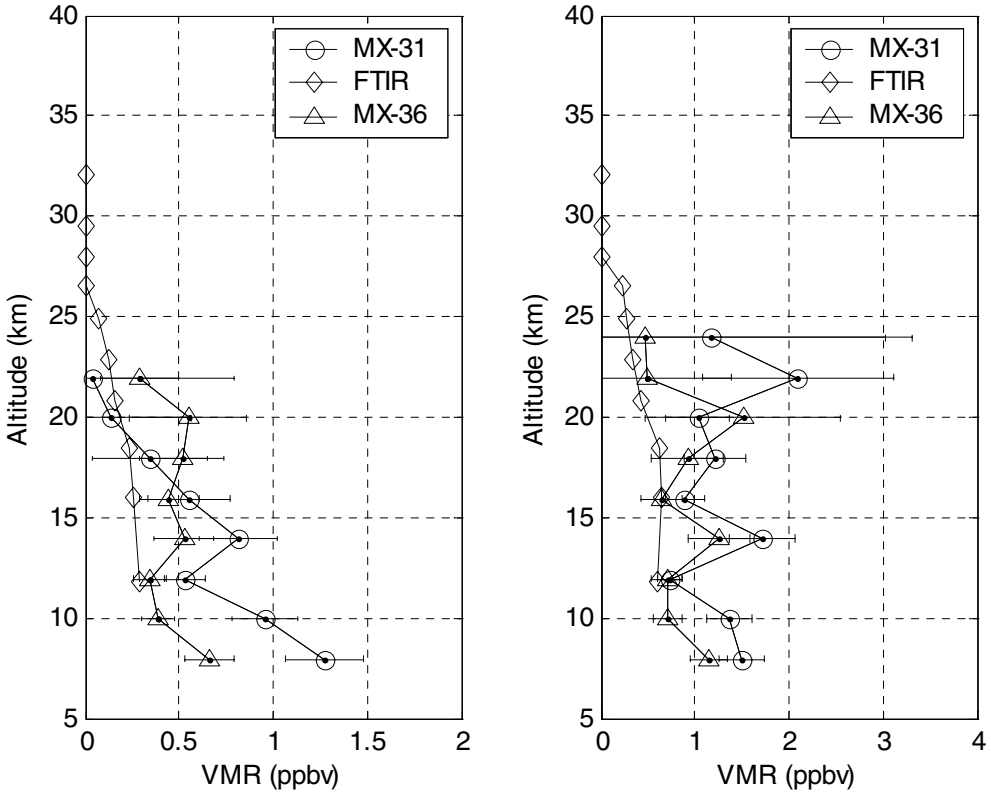

Fig. 12 VMR profiles for CFC-11 (left) and CFC-12 (right).

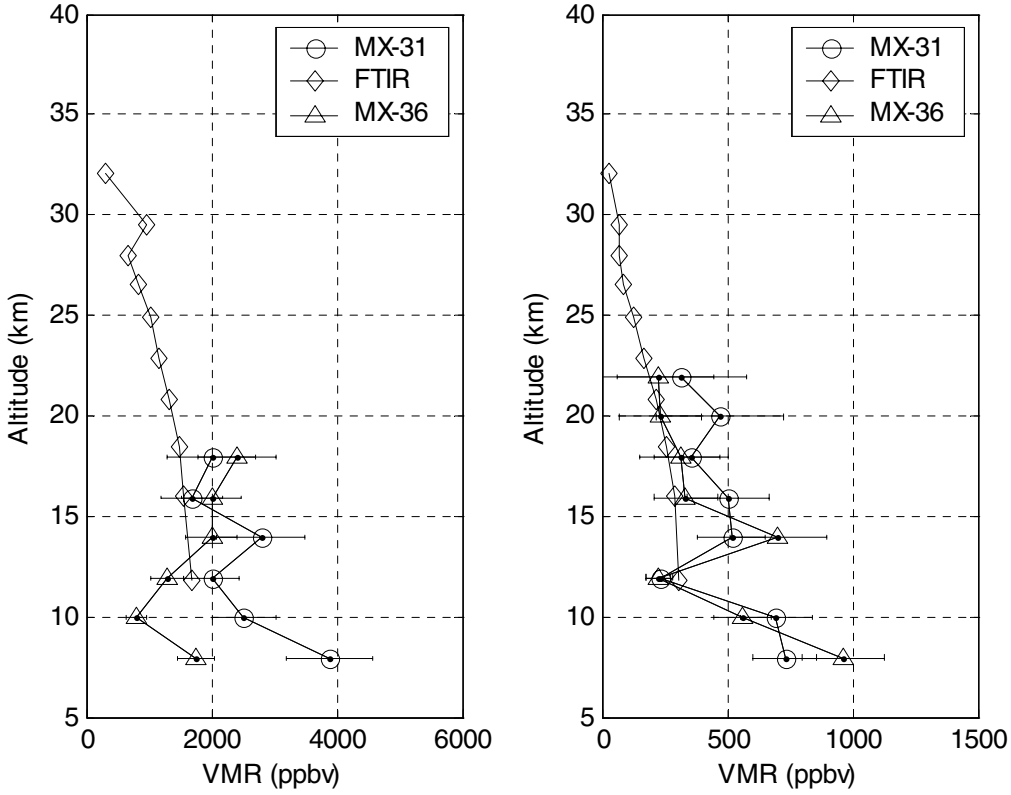

Fig. 13 VMR profiles for methane (left) and nitrous oxide (right).

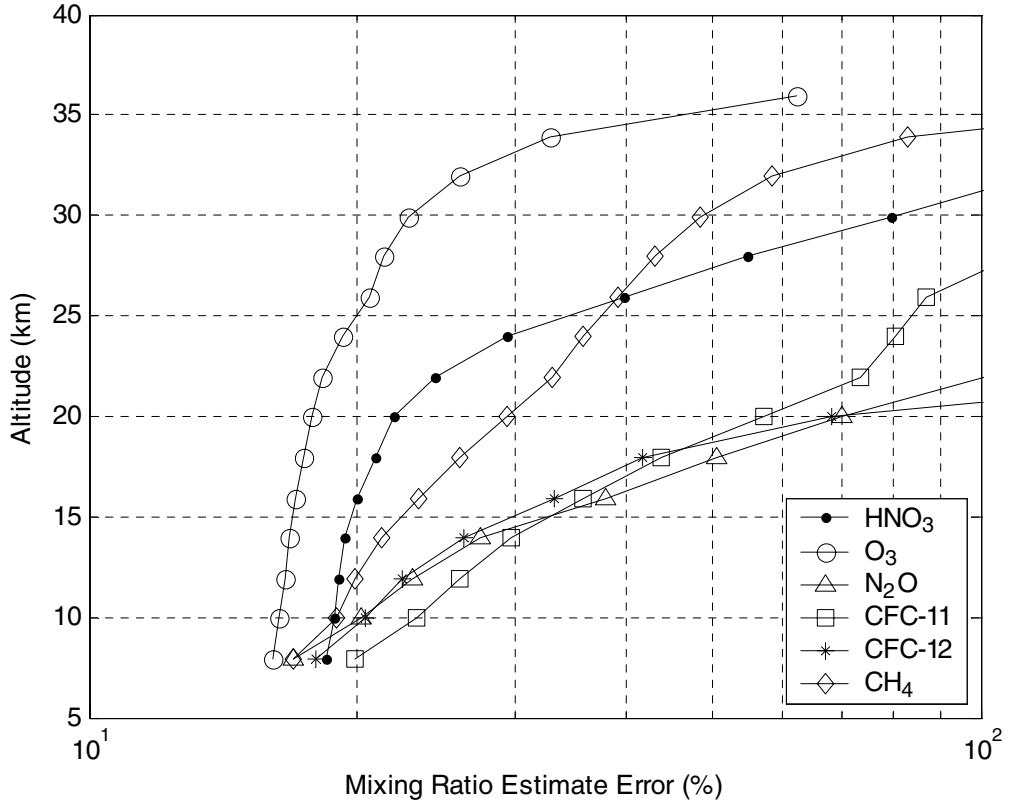

Fig. 14 Estimated mixing-ratio error by gas (as a percentage of the measured value).

TABLE 1. VMR results and expected (two sigma) error by gas for MX-31.

Altitude	HNO_3		O_3		N_2O		CFC-11		CFC-12		CH_4	
(km)	(ppbv)	% err	(ppmv)	% err	(ppmv)	% err	(ppmv)	% err	(ppmv)	% err	(ppmv)	% err
36.0	–	–	5.6	81.2	–	–	–	–	–	–	–	–
33.9	–	–	7.2	35.3	–	–	–	–	–	–	–	–
31.9	–	–	7.0	26.3	–	–	–	–	–	–	–	–
29.9	5.5	58.8	5.9	22.9	–	–	–	–	–	–	–	–
27.9	7.1	37.9	5.3	21.2	–	–	–	–	–	–	–	–
25.9	8.0	28.4	4.8	20.1	–	–	–	–	–	–	–	–
23.9	8.7	23.2	4.2	19.4	–	–	–	–	–	–	–	–
21.9	8.6	20.3	3.5	18.8	317.3	81.6	–	–	2.1	48.1	–	–
19.9	6.6	18.7	2.8	18.2	472.9	54.1	–	–	1.0	32.7	–	–
17.9	3.9	17.9	2.1	17.8	355.8	40.8	0.3	88.8	1.2	26.8	2.0	34.5
15.9	1.6	17.5	0.7	17.5	505.4	32.1	0.6	40.3	0.9	23.3	1.7	29.7
13.9	1.8	17.2	1.1	17.2	518.4	26.0	0.8	25.3	1.7	20.1	2.8	25.2
11.9	0.3	17.0	0.6	16.9	232.0	23.3	0.5	20.7	0.7	18.5	2.0	22.3
10.0	1.9	16.7	0.4	16.6	695.8	20.3	1.0	18.0	1.4	17.3	2.5	20.3
8.0	1.8	16.2	0.5	16.2	733.5	17.3	1.3	16.1	1.5	16.1	3.9	17.4

TABLE 2. VMR results and expected (two sigma) error by gas for MX-36.

Altitude	HNO_3		O_3		N_2O		CFC-11		CFC-12		CH_4	
(km)	(ppbv)	% err	(ppmv)	% err	(ppmv)	% err	(ppmv)	% err	(ppmv)	% err	(ppmv)	% err
38.0	–	–	–	–	–	–	–	–	–	–	–	–
36.0	–	–	9.4	62.4	–	–	–	–	–	–	–	–
33.9	–	–	5.5	33.0	–	–	–	–	–	–	–	–
31.9	–	–	7.1	26.1	–	–	–	–	–	–	–	–
29.9	4.1	79.5	4.7	22.8	–	–	–	–	–	–	–	–
27.9	5.9	54.8	2.6	21.5	–	–	–	–	–	–	–	
25.9	7.7	39.9	2.7	20.6	–	–	–	–	–	–	–	–
23.9	9.3	29.4	6.8	19.3	–	–	–	–	–	–	–	–
21.9	8.5	24.4	3.9	18.3	–	–	0.3	73.3	–	–	–	–
19.9	4.4	22.0	2.0	17.8	233.9	70.1	0.5	57.0	1.5	68.2	–	–
17.9	2.2	20.9	1.6	17.4	312.1	50.6	0.5	43.9	0.9	41.7	2.4	26.1
15.9	3.1	20.0	1.0	17.1	334.3	37.9	0.4	35.9	0.6	33.3	2.0	23.4
13.9	0.7	19.4	0.8	16.8	701.6	27.5	0.5	29.8	1.2	26.4	2.0	21.3
11.9	0.6	19.1	0.5	16.6	224.8	23.1	0.3	26.0	0.7	22.5	1.3	19.8
10.0	0.4	18.8	0.4	16.4	562.1	20.2	0.4	23.3	0.7	20.4	0.8	18.9
8.0	0.5	18.5	0.4	16.1	966.4	16.9	0.7	19.9	1.1	18.0	1.7	17.0

Figure 14 shows the results of this analysis. Only those points with errors of less than 100% have been reported in mixing-ratio profiles and tables. It should be noted that this analysis can only account for observable modelling errors that cannot be accounted for by changes in mixing ratio. By their very nature, such errors are unobservable and cannot be accounted for in any error analysis. Our errors are comparable with measurement errors reported for other HNO_3 observations, including those reported for MLS, with an accuracy quoted as approximately 40%, for the Limb Infrared Monitor of the Stratosphere (LIMS), estimated between 30% and 65% depending on altitude (Gille et al., 1984b), and for the Cryogenic Infrared Radiance Instrumentation for Shuttle (CIRRIS 1A), estimated between 21% and 41% (Bingham et al., 1997). Our error estimates are also consistent with balloon-based measurements of the CH_4 profile recorded in solar occultation and thermal emission by four independent grating spectrometer instruments during the Balloon Intercomparison Campaigns (BIC) in 1982 and 1983, reported by Zander et al. (1990), who estimate profile errors between 17% and 52% (two sigma) with an additional 11% line-strength and width uncertainty. Numerical values of VMR and two-sigma errors for our results are presented by instrument in Tables 1 and 2.

10 Conclusions

This paper presents vertical profile results for gases measured by emission radiometry during the MANTRA 1998 balloon mission. In an expansion from the previous single gas analysis of the nitric acid band, VMR for six gases are presented. Profiles are retrieved using a newly developed technique to recover gas VMR from low-resolution spectroscopic observations of the atmosphere and a revised calibration methodology. The model-based approach uses atmospheric and instrument models in a forward calculation to iterate for a globally optimal estimate of layer-by-layer gas amount using a least-mean-squares estimator. Results from the two instruments are broadly consistent and compare well with FTS and satellite data.

We report a nitric acid peak amount of 9 ppbv, recorded at 24 km, which is generally higher than the values measured by FTIR and MLS satellite instrumentation. However, we argue that the results and analysis presented here are an order of

magnitude more sensitive to local composition than comparable techniques, and other approaches may, in fact, smooth the vertical distribution of HNO_3, which, in turn, lowers the peak concentrations reported. Schneider et al. (1998) also report HNO_3 concentrations based on in situ sampling measurements that are generally higher than model calculations, advising that reactive nitrogen species may be underestimated—a conclusion consistent with our findings. Schneider's aircraft measurements also show significant horizontal and vertical structure in the HNO_3 field that is exhibited in profile results from both analysis procedures presented here. Our results also indicate similar structure present in the composition fields of other species, such as ozone. Although our conclusion is preliminary, there is evidence that climatological models may need to account for a kilometre-scale vertical variability using distributions of probable concentrations of atmospheric species at each model cell, rather than mean values, in order to model chemical dynamics correctly.

Our retrieval approach is directly applicable to a variety of other spectroscopic instruments where a global estimate of composition profile based on a large observation dataset is required. It is especially applicable to space-borne instruments where instrument resolution is often reduced in favour of a more robust design that is able to withstand launch and subsequent operation in a harsh space environment. In future work, we will apply this new approach to the retrospective analysis of flight data from previous radiometer missions that used the same instrument derivative and were flown during the past fifteen years in a similar location and season. We hope that this re-analysis of previous flight data on a consistent basis may yield information on the historical trends of nitric acid.

Acknowledgements

This research was funded by the Canadian Space Agency, the Meteorological Service of Canada, the Centre for Research in Earth and Space Technology and the Natural Sciences and Engineering Research Council of Canada. Special thanks go to Scientific Instrumentation Ltd., the other mission collaborators and all those who contributed to the success of the MANTRA 1998 balloon mission.

References

BINGHAM, G.E.; D.K. ZHOU, B.Y. BARTSCHI, G.P. ANDERSON, D.R. SMITH, J.H. CHETWYND and R.M. NADILE. 1997. Cryogenic infrared radiance instrumentation for shuttle (CIRRIS 1A) earth limb spectral measurements, calibration, and atmospheric ozone, nitric acid, CFC-12 and CFC-11 profile retrieval. *J. Geophys. Res.* **102**: D3, 3547–3558.

CHARTRAND, D. J.; J. DE GRANDPRÉ and J. C. MCCONNELL. 1999. An introduction to stratospheric chemistry. ATMOSPHERE-OCEAN, **37 (4)**: 309–367.

EVANS, W. F. J.; C. I. LIN and C. L. MIDWINTER. 1976. The altitude distribution of nitric acid at Churchill. *Atmosphere*, **14 (3)**: 172–179.

——; J.B. KERR, C.T. MCELROY and J.C. MCCONNELL. 1981. Simulation of nitrogen constituent measurements from the August 28, 1976, Stratoprobe III Flight. *J. Geophys. Res.* **86 (C12):** 12066–12070.

——; ——, ——, R.S. O'BRIEN and J.C. MCCONNELL. 1982a. Measurements of NO_2 and HNO_3 during a stratospheric warming at 54N in February 1979. *Geophys. Res. Lett*. **9 (4)**: 493–496.

——; ——, —— and J.C. MCCONNELL. 1982b. Simulation of the October 23, 1980, Stratoprobe flight. *Geophys. Res. Lett*. **9**: 223–226.

FOGAL P.F.; R.D. BLATHERWICK, F.J. MURCRAY and J.R. OLSON. 2005. Infra-red FTS measurements of CH_4, N_2O, O_3, HNO_3, HCl, CFC-11 and CFC-12 from the MANTRA balloon campaign. ATMOSPHERE-OCEAN, **43**: 351–359.

GALBALLY, I.E.; C.R. ROY, R.S. O'BRIEN, B.A. RIDLEY, D.R. HASTIE, W.F. J. EVANS, C.T. MCELROY, J.B. KERR, P. HYSON, W. KNIGHT and J.E. LABU. 1983. Measurements of the trace composition of the austral stratosphere: Chemical and meteorological data. Commonwealth Scientific and Industrial Research Organization, Australia, Aust. Div. Atmos. Res. Tech. Paper No. 1, pp. 1–31.

GILLE, J.C. and F.B. HOUSE. 1971. On the inversion of limb radiance measurements I: Temperature and thicknes. *J. Atmos. Sci.* **28**: 1427–1442.

—— and J. M. RUSSELL III. 1984a. The limb infrared monitor of the stratosphere: Experiment description, performance and results. *J. Geophys. Res.* **89** (D4): 5125–5140.

——; P.L. BAILEY, B.W. GANDRUD, J.M. RUSSELL, E.E. REMSBERG, L.L. GORDLEY, W.F.J. EVANS, H. FISCHER, A. GIRARD and J.E. HARRIES. 1984b. Accuracy and precision of the nitric acid concentrations determined by the limb infrared monitor of the stratosphere experiment on NIMBUS 7. *J. Geophys. Res.* **89** (D4): 5179–5190.

GOLDMAN, A.; F.S. BOMONO, F.P.J. VALERO, D. GOORVITCH and R.W. BOESE. 1981. Temperature dependence of HNO_3 absorption in the 11.3 micron region. *App. Optics*, **20**:172–175.

——; C.P. RINSLAND, A. PERRIN and J-M. FLAUD. 1998. HNO_3 line parameters: 1996 HITRAN update and new results. *J. Quant. Spectros. Radiat. Trans.* **60**(5): 851–861.

KUMER, J. B.; J. L. MERGENTHALER, A. E. ROCHE, R. W. NIGHTINGALE, G. A. ELY, W. G. UPLINGER, J. C. GILLE, S. T. MASSEE, P. L. BAILEY, M. R. GUNSON, M. C. ABRAMS, G. C. TOON, B. SEN, J.-F. BLAVIER, R. A. STACHNIK, C. R. WEBSTER, R. D. MAY, D. G. MURCRAY, F. J. MURCRAY, A. GOLDMAN, W. A. TRAUB, K. W. JUCKS and D. JOHNSON. 1996. Comparison of correlative data with HNO_3 version 7 from the CLAES instrument deployed on the NASA upper atmosphere research satellite. *J. Geophys. Res.* **101** (D6): 9621–9656.

MORELLI, D.W. 1998. The Interference Filter Handbook. OCLI-Optical Coating Laboratory,

MURCRAY, F.J.; F.H. MURCRAY C.P. RINSLAND, A. GOLDMAN and D.G. MURCRAY. 1987. Infrared measurements of several nitrogen species above the South Pole in December 1980 and November–December 1986. *J. Geophys. Res.* **92** (D11): 13,373–13,376.

NELDER J.A. and R. MEAD. 1965. A simplex method for function minimization. *Computer J.* **7** (4): 308-313.

OGSTON, S. 1991. Construction of a nitric acid profile from miniradiometer flight data. Environment Canada, Atmospheric Environment Service, Downsview, Canada, 26 pp.

PICK, D.R. and J.T. HOUGHTON. 1969. Measurements of atmospheric infrared emission with a balloon-borne multifilter radiometer. *Q. J. R. Meteorol. Soc*. **95**: 535.

QUINE B.M. and J.R. DRUMMOND. 2002. GENSPECT: A new generation line-by-line code with a bounded interpolation accuracy. *J. Quant. Spectros. Radiat. Trans.* **74**: 147–165.

ROSELLI, N.J.; R.S. O'BRIEN and W.F.J. EVANS. 1977. Stratospheric ozone from the inversion of balloon-borne thermal emission measurements of the 9.6μ band. APRB 83 X 20, Atmospheric Environment Service, 47 pp.

ROTHMAN, L.S.; A. BARBE, D. CH. BENNER, L.R. BROWN, C. CAMY-PEYRET, M.R. CARLEER, K. CHANCE, C. CLERBAUX, V. DANA, V. MALATHY-DEVI, A. FEYT, J.M. FLAUD, R.R. GAMACHE, A. GOLDMAN, D. JACQUEMART, K.W. JUCKS, W.J. LAFFERTY, J-Y. MADIN, S.T. MASSIE, V. NEMTCHINOV, D.A. NEWNHARM, A. PERRIN, C.P. RINSLAND, J. SCHROEDER, K.N. SMITH, M.A. SMITH, K. TANG, R. A. TOTH, J. VANDER AUWERA, P. VARANASI and K. YOSHINO. 2003. The HITRAN molecular spectroscopic database; edition of 2000 through 2001. *J. Quant. Spectros. Radiat. Trans.* **82**: 5–44.

SALBY, M.L. 1996. *Fundamentals of Atmospheric Physics*. Academic Press, 624 pp.

SANTEE, M. L.; G. L. MANNEY, N. J. LIVESEY and W. G. READ. 2004. Three-dimensional structure and evolution of stratospheric HNO_3 based on UARS microwave limb sounder measurements. *J. Geophys. Res.* **109**: D15306, doi: 10.1029/2004JD004578.

SCHNEIDER, J.; F. ARNOLD, V. BURGER, B. DROSTE-FRANKE, F. GRIMM, G. KIRCHNER, M. KLEMM, T. STILP, K.-H. WOHLFROM, P. SIEGMUND and P. VAN VELTHOVEN. 1998. Nitric acid in the upper atmosphere and lower stratosphere at mid-latitudes: new results from aircraft-based mass spectrometric measurements. *J. Geophys. Res.* **103** (D19): 25337–25343.

STRONG, K.; G. BAILAK, D. BARTON, M.R. BASSFORD, R.D. BLATHERWICK, S. BROWN, D. CHARTRAND, J. DAVIES, J.R. DRUMMOND, P.F. FOGAL, E. FORSBERG, R. HALL, A. JOFRE, J. KAMINSKI, J. KOSTERS, C. LAURIN, J.C. MCCONNELL, C.T. MCELROY, C.A. MCLINDEN, S.M.L. MELO, K. MENZIES, C. MIDWINDER, F.J. MURCRAY, C. NOWLAN, R.J. OLSON, B.M. QUINE, Y. ROCHON, V. SAVASTIOUK, B. SOLHIEM, D. SOMMERFELDT, A. ULLBERG, S. WERCHOHLAD, H. WU and D. WUNCH. 2005. MANTRA - A balloon mission to study the odd-nitrogen budget of the stratosphere. *Atmosphere-Ocean*, **43**: 283–299.

TOTH, R. A.; L. R. BROWN, and E. A. COHEN. 2003. Line intensities of HNO_3. *J. Mol. Spectros.* **218**: 151–168.

ZANDER, R.; N. LOUISNARD and M. BANGHAM. 1990. Stratospheric methane concentration profiles measured during the balloon intercomparison campaigns. *J. Atmos. Chem.* **10**: 145–158.